Annals of Glaciology (2017), Page 1 of 11 doi: 10.1017/aog.2017.11

Stable isotope (δD–$\delta^{18}O$) relationships of ice facies and glaciological structures within the mid-latitude maritime Fox Glacier, New Zealand

John R. APPLEBY,[1] Martin S. BROOK,[2] Travis W. HORTON,[3] Ian C. FULLER,[1] Katherine A. HOLT,[1] Duncan J. QUINCEY[4]

[1]*Institute of Agriculture and the Environment, Massey University, Palmerston North, New Zealand*
[2]*School of Environment, The University of Auckland, Auckland, New Zealand.*
E-mail: m.brook@auckland.ac.nz
[3]*Department of Geological Sciences, University of Canterbury, Christchurch, New Zealand*
[4]*School of Geography, University of Leeds, Leeds, UK*

ABSTRACT. Relationships between stable isotopes (δD–$\delta^{18}O$), ice facies and glacier structures have hitherto gone untested in the mid-latitude maritime glaciers of the Southern Hemisphere. Here, we present δD–$\delta^{18}O$ values as part of a broader study of the structural glaciology of Fox Glacier, New Zealand. We analyzed 94 samples of δD–$\delta^{18}O$ from a range of ice facies to investigate whether isotopes have potential for structural glaciological studies of a rapidly deforming glacier. The δD–$\delta^{18}O$ measurements were aided by structural mapping and imagery from terminus time-lapse cameras. The current retreat phase was preceded by an advance of 1 km between 1984 and 2009, with the isotopic sampling and analysis undertaken at the end of that advance (2010/11). Stable isotopes from debris-bearing shear planes near the terminus, interpreted as thrust faults, are isotopically enriched compared with the surrounding ice. When plotted on co-isotopic diagrams (δD–$\delta^{18}O$), ice sampled from the shear planes appears to show a subtle, but distinctive isotopic signal compared with the surrounding clean ice on the lower glacier. Hence, stable isotopes (δD–$\delta^{18}O$) have potential within the structural glaciology field, but larger sample numbers than reported here may be required to establish isotopic contrasts between a broad range of ice facies and glacier structures.

KEYWORDS: glacier hydrochemistry, mountain glaciers, structural glaciology

INTRODUCTION

Delineating relationships between ice facies, structures and debris entrainment has proven to be an area of emerging interest for many researchers over the past two decades. This includes work at a range of glacier settings: Variegated Glacier, Alaska (Sharp and others, 1994), Iceland (Cook and others, 2010; Phillips and others, 2013), Greenland (Larsen and others, 2010), Svalbard (Lovell and others, 2015a, b), European Alps (Hubbard and others, 2000; Goodsell and others, 2005; Jennings and others, 2014) and Sweden (Glasser and others, 2003; Moore and others, 2013). Previous research has focused especially on structural controls on debris transport and entrainment within high-Arctic polythermal glaciers (Hambrey and others, 1999; Lovell and others, 2015a), with the analysis of the structural evolution of maritime alpine glaciers relatively rare (Appleby and others, 2010; Phillips and others, 2013). Nevertheless, all of these studies have contributed to knowledge of strain histories and mechanisms of deformation, which is important in understanding the controls on foliation, folding and thrusting, and debris entrainment, transport and deposition (Moore and others, 2013). A potential approach of investigating patterns and mechanisms of deformation within glaciers is the use of stable isotopes δD-$\delta^{18}O$ (Glasser and Hambrey, 2002). This is because water undergoes isotopic fractionation on freezing, and so combined measurements of δD and $\delta^{18}O$ provide the opportunity to distinguish between isotopically unmodified englacial or meteoric ice and isotopically modified basal ice (Souchez and Jouzel, 1984). Uplift of basal ice is thought to occur through bulk thickening, folding or thrusting (Alley and others, 1997). Thrusting (and folding) in particular can juxtapose ice and sediment facies formed in very different englacial or basal environments, and may thus be responsible for the appearance of debris layers of basal origin overlying englacial ice of meteoric origin (Moore and others, 2013). In theory, combined δD and $\delta^{18}O$ measurements make it possible to distinguish between isotopically unmodified englacial ice and isotopically modified basal ice by plotting values of δD and $\delta^{18}O$ (in ‰ relative to Vienna Standard Mean Ocean Water, VSMOW) on a co-isotopic diagram (Souchez and Jouzel, 1984). Samples of glacier ice that have not undergone refreezing as might, for example, basal ice or superimposed ice (Benn and Evans, 2010), should lie along the same regression line as precipitation on a δD–$\delta^{18}O$ covariance diagram. Ice that has undergone refreezing should produce a regression line with a lower slope, depending on the initial isotope values of the melted ice at the onset of regelation (Souchez and Jouzel, 1984; Glasser and Hambrey, 2002).

Despite this theory, δD–$\delta^{18}O$ relationships with glacier structures and ice facies have hitherto remained untested in the mid-latitude maritime glaciers of the Southern Hemisphere. Based on prior studies (Glasser and Hambrey, 2002), the local meteoric water line (LMWL) can be assumed to represent unmodified meteoric ice, which inherits its isotopic signature of precipitation, compared with ice

facies, which have potentially undergone melting and refreezing. Thus, we hypothesize that comparison of the co-isotopic composition of debris-bearing glacier ice with the LMWL could potentially help constrain the debris entrainment process and structural deformation of Fox Glacier, New Zealand. This is a temperate maritime glacier on the western flank of New Zealand's Southern Alps. Recent observations by Appleby and others (2010) part-characterized the pattern of brittle and ductile structures developed on the glacier surface, and proposed that thrusting elevates basal debris along shear planes to the surface toward the glacier terminus during periods of advance. While the weight of evidence pointed to thrusting, the high ablation rates (>0.13 m d^{-1}, Purdie and others, 2008) on the lower glacier meant it was difficult to demonstrate large displacements along potential thrust planes. Here, we characterize in more detail from névé to terminus the surface structure of Fox Glacier, and sample δD and $\delta^{18}O$ at 94 points on the glacier surface, across a range of different ice facies. We also acquired imagery from a time-lapse camera positioned in front of the terminus of Fox Glacier to observe the structural evolution of the terminus over a 3-week period during the peak of the ablation season. Taken together, this has provided an opportunity to test general theories regarding the origin of different glacigenic structures, during the 2010/11 survey period. The survey period followed the end of a two decade period (1984–2009) during which the glacier advanced 1 km down-valley, and thickened substantially (Purdie and others, 2014).

STUDY AREA

Fox Glacier (43°30′S; 170°10′E) is a 12.5 km long (in 2016; but 12.9 km long during the study in 2010/11) valley glacier, and is a sensitive indicator of climatic variations across a range of timescales from millennia-long glaciations to decadal and interannual variations (Purdie and others, 2014). The 36 km^2 glacier is on the western side of the Southern Alps (Fig. 1), descending from the western face of Mount Tasman at ~2800 m a.s.l.. The broad high-elevation névé funnels ice down a steep narrow tongue, and terminates below 300 m a.s.l., far below its equilibrium line altitude (ELA) of ~1830 m a.s.l. (in 2010/11). The steep long-profile, broad accumulation area and narrow valley means the terminus responds rapidly to climate-induced changes in mass balance, of the order of 9 years (Purdie and others, 2008). The Main Divide of the Southern Alps intercepts the dominant westerly airflow, resulting in up to 15 m w.e. a^{-1} precipitation in the accumulation area of Fox Glacier (Coates and Chinn, 1999). Thus, the overall catchment geometry and steep topography exert a control on the pattern of ice flow and glacier structures, which has been investigated by Purdie and others (2008) and Appleby and others (2010), although these studies were limited to the lower part of Fox Glacier. Ice is channeled rapidly down the upper icefall, before slowing where the valley slope decreases in a zone termed Victoria Flat (Herman and others, 2011). The valley long profile then steepens down-glacier, and ice extends and flows rapidly down the lower icefall toward the terminus (Fig. 1).

Although the overall recent trend of Fox Glacier (and nearby Franz Josef Glacier) has been one of retreat, there have been significant periods of re-advance during the 20th and early 21st centuries (Purdie and others, 2014). The most recent advance phase of 1 km (ending in 2009) provided a rare and ideal opportunity for the study of deformational structures and debris transfer during a glacier advance (see Appleby and others, 2010). While measurements of these glacier length changes have been made with GPS, any ice-marginal moraines that are deposited are highly transient landforms, being typically destroyed by erosion from the proglacial river (Brook and Paine, 2012; Purdie and others, 2014).

METHODS

Glacier structures

The structural glaciology of Fox Glacier was established by structural mapping of ~12 km-long surface based on overlapping aerial photographs. Structures were identified on the photographs according to their dimensions, orientation and cross-cutting relationships. In addition, structures were identified in the field and mapped on the ground using a compass/clinometer. Field data were collected from a series of transverse profiles from the accumulation zone to the terminus, using a similar survey pattern to that detailed in Goodsell and others (2005). Data collected were foliation, primary stratification, various crevasse systems and crevasse traces. All structural glaciological data and description of the sequential development of glacier structures followed standard structural geological notation outlined in Goodsell and others (2005). Hence, structures were coded from S_0 upwards, based on the presumed order of formation, in accordance with structural geology conventions (Hambrey and others, 2005).

To monitor the temporal evolution of structures at the terminus, a sequence of daily images was collected from a time-lapse camera installed on the early 20th-century moraine (Wardle, 1973) on the south side of the proglacial zone, obliquely facing the glacier terminal face. This is a slightly elevated position above the braided proglacial valley floor. The images were used to capture a temporal record of structural glaciological processes at the terminus during a phase of glacier advance. The imagery was captured over a period of 3 weeks toward the end of the 2010 ablation season (from 22 March 2010 to 11 April 2010). This provided important glaciological context for the oxygen isotope data gathered during the present study, as well as allowing a comparison with the observations and measurements reported in the investigation of Appleby and others (2010).

Ice facies

Ice facies were identified and classified according to their physical characteristics following Goodsell and others (2005) and Hubbard and others (2009). Firn and englacial ice was classified at three main locations: firn in the accumulation zone, Victoria Flat (between the upper and lower icefalls) and in the lower glacier (between the lower icefall and terminus). Ice was also classified and sampled in the basal zone, in an accessible point on the north side of Victoria Flat.

Stable isotopes

Isotope samples were collected at a range of sites, which corresponded to the locations where ice facies were classified in situ. This allowed scope for elucidating possible relationships

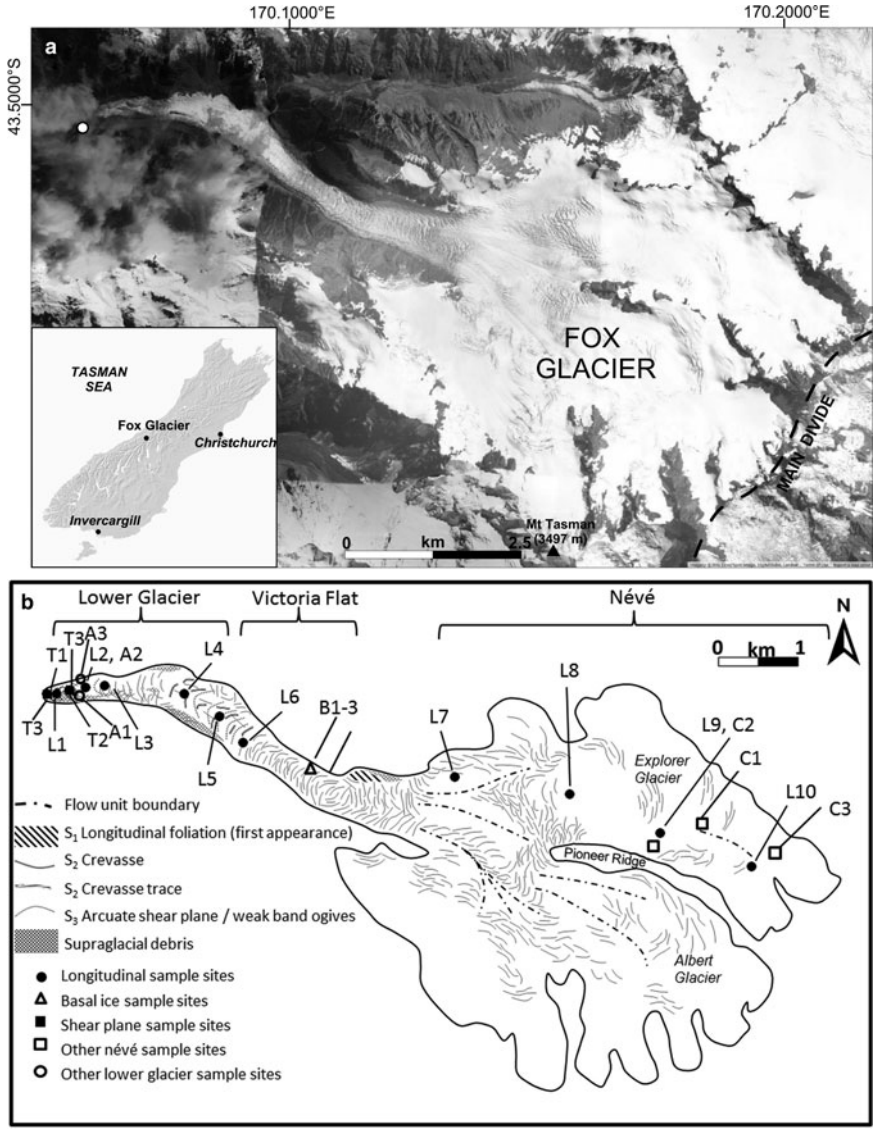

Fig. 1. (a) Image and inset location map of Fox Glacier, as well as Invercargill, the closest monthly precipitation (including δD–$\delta^{18}O$) LMWL data from the IAEA's GNIP database. Position of time-lapse camera in front of the terminus is shown by the white circle. Image courtesy of ArcGIS Online World Imagery. (b) Summary structural glaciological map of Fox Glacier, and sampling locations for stable isotopes.

between stable isotopes and ice facies and/or structures (Fig. 1). The stable isotope sample sites included ice presumably of englacial origin, from a longitudinal transect along the glacier centerline, transverse transects across the névé to collect firn, basal ice along the northern glacier margin and ice from arcuate shear planes toward the terminus, previously assumed to include regelation ice (Appleby and others, 2010). Samples were collected according to the methods outlined in Glasser and others (2003), over a 2-day period during February 2011. At each sample site, firn or ice was removed from the glacier using an ice screw at 5–20 cm depth to avoid surface melting and stored in air-tight plastic bottles in the shade to prevent evaporation. The altitude and location of each sample site was logged and the ice facies characterized. Along the longitudinal transect, sampling locations were irregularly spaced because parts of the upper and lower icefalls were largely inaccessible.

Samples were analyzed at the University of Canterbury using the Thermo Scientific Finnigan thermal combustion elemental analyzer coupled to a Thermo Scientific Delta V Plus isotope ratio spectrometer via a Conflo III gas distribution system. Operating conditions for the elemental analyzer were a reactor temperature of 1420°C, a gas chromatography column temperature of 40°C, with a 99.999% He continuous flow rate of ~110 ml min^{-1}. Each sample including duplicate analyses was analyzed four times, and data were corrected using a 2-point normalization (i.e. stretch and shift) to the VSMOW-SLAP (VSMOW-Standard Light Arctic Precipitation; Gonfiantini, 1978) scale. Using this process, the δD values were accurate to <1.0‰ and the $\delta^{18}O$ values are accurate to <0.2‰. All regressions were calculated in IBM-SPSS v23 and plotted in Grapher 11.

The International Atomic Energy Agency (IAEA) provides details of isotopic contents (including δD–$\delta^{18}O$) of composite monthly precipitation on their Global Network of Isotopes in Precipitation (GNIP) database. The closest station to Fox Glacier is at Invercargill (46°24′S, 168°24′E, 5 m a.s.l.) at the southern tip of the South Island, and monthly values from this database (between 1977 and 2008) were used for comparison with δD–$\delta^{18}O$ data from Fox Glacier. The GNIP data are expressed as the per mil (‰) deviation of the isotope ratio from the primary measurement standard. The measurements reported in GNIP have a long-term precision of ~±0.1‰ for $\delta^{18}O$ and ±0.8‰ for δD, at one SD (IAEA,

1992). As the data were collected at sea level, they provide no information on the altitudinal variation of isotopic composition.

RESULTS

Structural glaciology

Glacier structures identified in the field and on the aerial photographs are summarized in Table 1. In a sense, the glacier typifies the structural patterns observed in many other alpine glaciers (Goodsell and others, 2005), insofar as it displays folding of primary stratification, and zones of crevasses in response to tension. In the névé, planar primary stratification (S_0) is visible in crevasse walls (Fig. 2a) undergoing firnification. Flow unit boundaries are also identifiable in the névé (Fig. 2b), each of which delineates the boundary between different subaccumulation basins. There is no evidence of debris septa developing, or any debris emerging, as this is above the ELA. The flow unit boundaries converge at the top of the upper icefall. Individual flow units cannot be traced any further down-glacier than this point. As ice is then channelized into the valley trough, and primary stratification (S_0) is compressed and attenuated into a series of folds whose axes are aligned along glacier, forming steeply dipping (80°–90°) fold limbs (Fig. 2c), designated longitudinal foliation (S_1). Hence, both S_0 and S_1 structures are end members of the same continuum.

Several different patterns of open crevasses (S_2) were observed across the glacier, and these relate directly to the orientation of the stress field within the glacier in a given time and space. Crevasses traces generally parallel adjacent open crevasses, indicating they are both forming along the stress–strain continuum, while other crevasse traces cross-cut the prevailing (open) crevasse pattern. Transverse crevasses, representing extensional flow, are first visible in the accumulation basins, where englacial ice and firn starts flowing toward the upper icefall (Fig. 2a, Table 1). Within both the upper and lower icefalls, crevasse morphology becomes obscured due to rapid surface melt (~13 cm d^{-1}; Purdie and others, 2008), and sérac development on the intervening ablating ice units. A series of crevasses and crevasse traces (S_2) are formed within the channelized section of the glacier in Victoria Flat, a ~2.5 km long zone of subdued ice surface topography between the upper and lower icefalls. Weak band ogives were previously identified in this zone (Appleby and others, 2010), and form an arcuate pattern on the surface. Longitudinal crevasses also occur in Victoria Flat, due to lateral extension, given in the wider valley floor width. Splaying and chevron crevasses also occur here at the glacier margins.

Toward the terminus, both chevron, splaying and longitudinal crevasses can be identified (Fig. 2d), with arcuate shear planes (S_3) forming up-glacier dipping structures close to the terminus (Figs 2e–g). These shear planes are perpendicular and subperpendicular to ice flow, and dip at a low angle (15–25°) up-glacier, extending from the subglacial zone to the surface. At the surface, distinct hanging wall and footwall blocks can be identified (Fig. 2e). The shear planes appear to represent thrust faults, accommodating longitudinal shortening of the glacier, and truncate earlier structures. The temporal evolution of the shear planes was captured by time-lapse imagery in Figure 3. Over the period of observations, sequential images indicate that shearing along distinct planes occurs at the terminus. This is evident from the material being extruded from ice emerging along shear planes in the terminal ice cliff. This material then falls and flows under gravity, forming low ridges (0.5 m high) of morainic deposits, which are rapidly eroded by meltwater and rainfall.

Ice facies

Four different firn/ice facies were identified and sampled in the field, and are summarized in Table 2. Coarse-crystalline, granular firn (Table 2) was ubiquitous across the accumulation zone, visible in pits and the walls of open crevasses. The englacial ice facies (Table 2) was observed at Victoria Flat, the lower glacier, and along a longitudinal profile down the glacier centerline. The englacial facies has an omnipresent stratification at centimeter to decimeter scales and takes the form of intercalated layers of bubble-rich and bubble-poor ice. This layering is visible on the glacier surface, and can be traced across the walls of crevasses by minor color changes. Englacial facies is for the most part, clean ice; however, occasional suspended grains and small clots of fine sediment are sometimes visible.

A dispersed ice facies (Table 2) was observed at the glacier bed at the northern margin of Victoria Flat, where a meltwater stream from the tributary Victoria Glacier catchment allows entrance to the subglacial zone via an ice cave. This facies clearly contrasted with the clean englacial ice. It

Table 1. Summary of principal glaciological structures within Fox Glacier

Planar glaciological structures	Description	Interpretation
S_0*	Primary stratification	Firnification processes in the accumulation zone producing original layering
S_1*	Longitudinal foliation	Folding of S_0, eventually leading to isoclinal fold limbs that parallel ice flow; intersect the surface, long, linear pervasive layered structures; alternating, discontinuous layers of bubble-rich and bubble-free white and blue ice
S_2	Crevasses and crevasse traces	Crevasses due to local extension; transverse crevasses in upper icefall; longitudinal crevasses in Victoria Flat; chevron and splaying crevasses toward snout; crevasse traces either closed crevasses, or extensional veins of existing crevasses
S_3	Transverse arcuate	Shear planes in lower glacier, laterally continuous, up-glacier dipping (<25°), cross-cutting foliation (S_1) and crevasse traces (S_2); related to longitudinal compression
N/A	Flow unit boundary	Junction separating flow units in accumulation basin; recognized by discordant structures either side and a narrow trough in the field

* S_0 and S_1 represent end members of a structural continuum.

Fig. 2. Details of typical glaciological structures at Fox Glacier. (a) S_0 primary stratification of firn in the accumulation zone. Note the development of transverse crevasses as ice accelerates down the upper icefall. (b) Flow unit boundary at confluence of Explorer Glacier (left) and Albert Glacier (right), below Pioneer Ridge. (c) Modified primary stratification (S_0) forming longitudinal foliation (S_1) exposed as isometric folds (hashed lines). (d) Open splaying crevasses (S_2) cutting across longitudinal foliation (S_0), both truncated by arcuate shear planes (S_3), interpreted as listric thrust faults. (e) Clayey material extruded at the surface along an S_3 arcuate shear plane. (f and g) Arcuate shear planes (S_3) at the terminus cross-cutting all existing structures, such as crevasses, crevasse traces.

consists of decimeters thick, typically bubble-free ice containing diamicton that varied in concentration and character (but typically <1%). Indeed, particle concentration and type varied, with suspended grains and clots of silt-sized fine sediment that occasionally form thin <2 cm bands. Rarely, clasts are entrained within the ice.

The third ice facies encountered is associated with the shear planes below the lower icefall toward the terminus. This facies, evident as shear plane ice, contrasts strongly with the overlying and underlying clean englacial facies. Indeed, the shear plane facies varies from clear, bubble-free ice, to dense white clouds of bubbles. It has a moderate debris content (<10%), largely consisting of a clayey laminae and rare, suspended rounded pebbles. The clayey laminae have a strong linear component, characterized by strong alignment of grains or clots of fine sediments. This facies typically forms planar, 3–5 cm thick bands, dipping up-glacier.

Stable isotopes

The GNIP stable isotope data from Invercargill are presented on a δD–$\delta^{18}O$ co-variate plot in Figure 4, and shows a linear relationship described by a least-squares regression $\delta D = 7.726\delta^{18}O + 7.355$, $R^2 = 0.92$, $p < 0.0001$). These data probably hide considerable intraannual precipitation variability; however, they indicate the slope of the LMWL at Invercargill is 7.72, conforming closely to the slope of the global meteoric water line (GMWL). As the data are collected at Invercargill close to sea level, they provide no information on altitudinal variability of snowfall on the glacier, which descends from the Main Divide of the Southern Alps to ~300 m a.s.l. The 94 samples from Fox Glacier are also included on the plot, and despite the range in glacier surface altitude, the data and slope of the regression (6.81) closely correspond to the Invercargill LMWL and the GMWL.

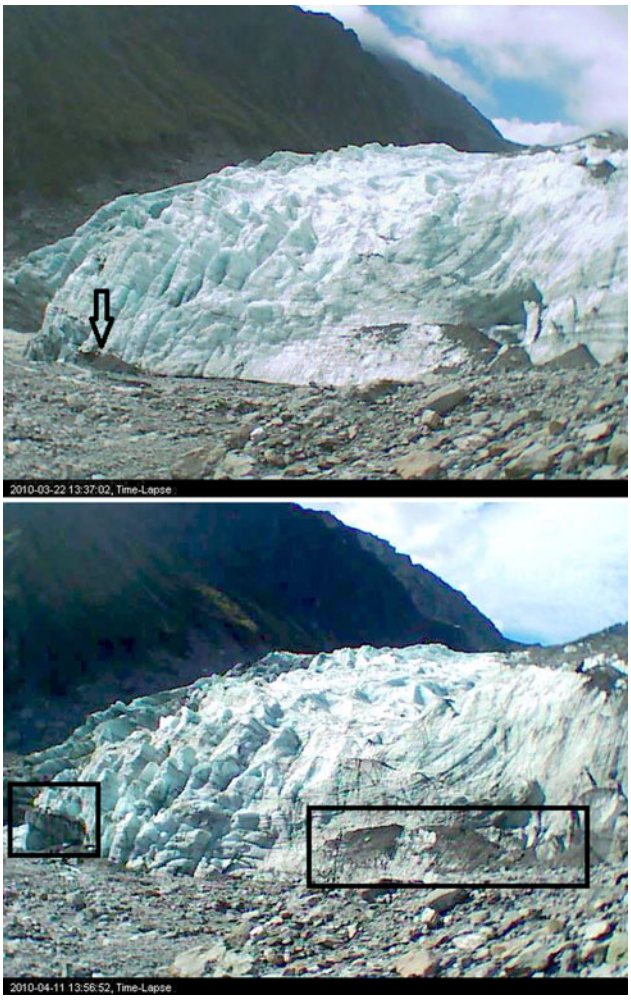

Fig. 3. Two time-lapse images from the terminus of Fox Glacier from 22 March 2010 (image 1) and 11 April 2010 (image 2). Regarding the structural glaciology, a small (<2 m high) moraine is formed by bulldozing of proglacial sediment in the center of the terminus (arrowed in image 1). Sediment is also being extruded from low-angle shear structures at the far left and right of the images (boxed areas in image 2).

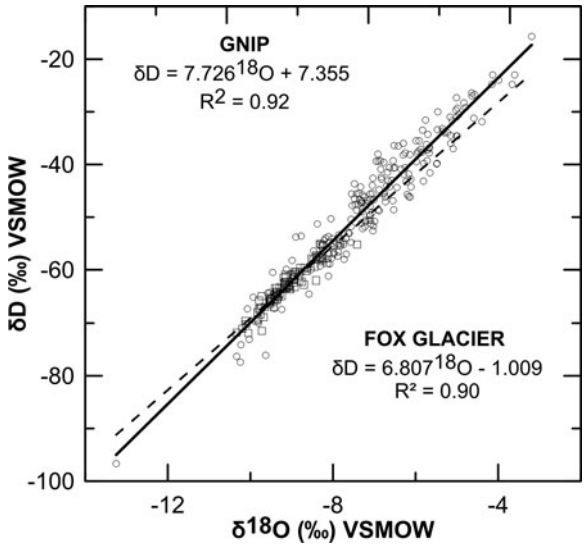

Fig. 4. Co-isotope scatterplot (δD–δ^{18}O) of monthly precipitation recorded at Invercargill, South Island, New Zealand from the IAEA's GNIP database between 1977 and 2008 circles (solid regression line); also included on the plot are all data from this study (squares) and associated linear regression (hashed line).

Mean and SDs of δD and δ^{18}O for each of the sample facies are presented in Figure 5 and Table 2. As is expected, there is substantial overlap between some of the sample facies. The firn facies from the névé appears to show more positive isotope values compared with all other datasets, while the englacial facies from Victoria Flat is the most clustered. Absolute δD values range between −54.92 and −71.83‰, with an overall mean of −62.54‰. Absolute δ^{18}O values range between −7.97 and −10.33‰, with an overall mean of −9.06‰. For both δD and δ^{18}O, the englacial ice facies sampled on the lower glacier displays the highest mean values (δ^{18}O = −9.74‰, δD = −67.30‰), while the firn facies in the névé displays the lowest mean values (δ^{18}O = −8.48‰; δD = −58.78‰). There does appear to be a degree of heterogeneity between different englacial facies, with the englacial ice facies sampled at Victoria Flat closest isotopically to the firn facies from the névé. The δD–δ^{18}O relationships for different facies are explored further in the co-isotopic scatterplots in Figure 6. None of the stable isotope measurements are as heavy as the precipitation-derived data at Invercargill (Fig. 5).

The basal ice facies was sampled directly at the northern lateral margin of the glacier, but there appears to be no clear differentiation between δD–δ^{18}O relationship for this ice facies and the regression slopes of englacial or meteoric (i.e. firn) facies. Indeed, the basal ice facies δD and δ^{18}O

Table 2. Description of ice facies, sample zones and summary statistics of sampled δD–δ^{18}O stable isotopes

Ice facies/proposed origin	Physical characteristics	Sample locations	δ^{18}O ‰ VSMOW	δD ‰ VSMOW
Firn/meteoric	Coarse-crystalline, granular firn	Accumulation zone	−8.48 ± 0.32	−58.78 ± 2.90
Englacial/meteoric ice	Debris-free to very-low debris content; white, opaque appearance; bubble-rich; alternations of bubble-rich and bubble-poor ice	Victoria Flat	−8.70 ± 0.31	−60.62 ± 1.92
		Lower glacier	−9.74 ± 0.40	−67.30 ± 3.12
		Longitudinal profile	−8.93 ± 0.64	−61.89 ± 4.53
Dispersed/basal ice	Decimeters thick; bubble-free ice containing diamicton that varies in concentration (typically <1%)	Northern margin	−8.95 ± 0.44	−61.68 ± 2.89
Shear planes, Possible thrusting	Clear, bubble-free to dense white clouds of bubbles; low debris content (<10%), largely consisting of clayey laminae and occasional suspended rounded pebbles	Below lower icefall	−9.41 ± 0.26	−64.32 ± 2.44

Physical characteristic descriptions follow Hubbard and others (2009) and Fierz and others (2009)

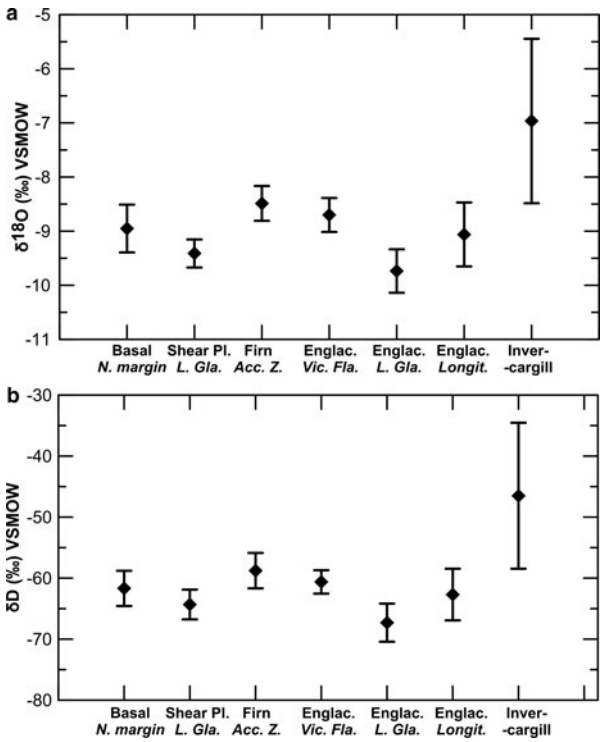

Fig. 5. Summary mean and SD of (a) δD and (b) δ^{18}O samples at Fox Glacier for different sampling locations and ice facies.

data are clustered tightly around a regression slope of 6.33 (Fig. 6). The δD–δ^{18}O relationship of the shear plane ice facies indicates that this facies appears to show a slightly different stable isotope signal when compared with other surrounding englacial ice facies on the lower glacier (Fig. 6). In particular, the shear plane ice facies is isotopically heavier than the surrounding englacial facies.

Nevertheless, the scatter of data and range of δD–δ^{18}O relationships displayed in Figure 6 for the different ice facies are difficult to distinguish clearly. All the regression slopes are close to the LMWL and GMWL, apart from the englacial facies sampled at Victoria Flat and basal ice facies (regression slopes of 5.065 and 6.330, respectively). A contrast does exist between the regression slopes of firn (7.869) and the englacial ice facies (5.065) sampled at Victoria Flat, but the reasons for this are unclear, given they are both presumably of meteoric origin. Nevertheless, all of the regressions confirm strong, statistically significant ($p < 0.001$) relationships between δD and δ^{18}O (Table 3), as confirmed by the R^2 and F-statistic values. The 95% confidence ranges in b_1 (δ^{18}O) coefficients (Table 3) could be used to determine whether significantly different relationships exist as a function of ice facies. However, the b_1 ranges for each facies overlap, which suggests that the relationships are not significantly different. Nevertheless, a t test does reveal a statistically significant difference (at $p < 0.01$) between more positive isotopic values in the shear plane ice facies than the surrounding clean englacial facies on the lower glacier, for both δ^{18}O and δD.

Variations in the δD–δ^{18}O relationships are also apparent with altitude along Fox Glacier, using the longitudinal englacial facies and firn data from along the glacier centerline (Fig. 7), although the results do not exhibit uniform spatial patterns of heavier or lighter isotopes. A possible trend of a more positive isotopic signal with increasing altitude into the névé does occur, but the altitudinal scatter of δD–δ^{18}O data becomes increasingly heteroscedastic around the regression toward the glacier terminus.

DISCUSSION

The pattern and distribution of observed glacier structures at Fox Glacier is typical of those reported from other valley

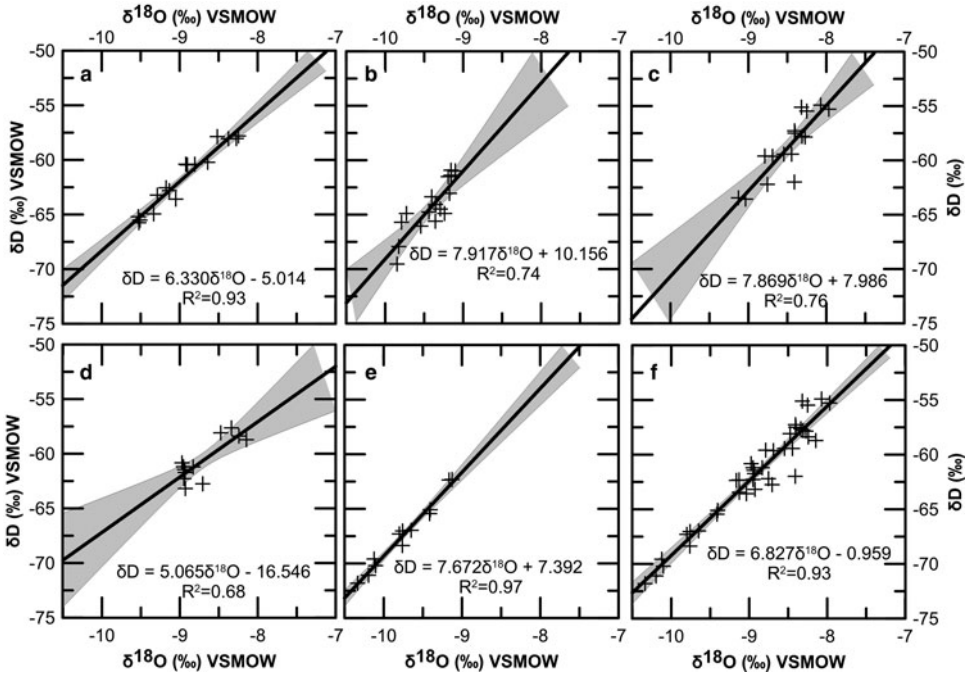

Fig. 6. Co-isotopic scatterplots of oxygen and deuterium (δ^{18}O and δD) from the following ice facies/sampling zones at Fox Glacier: (a) basal ice; (b) shear plane ice below the lower icefall; (c) firn from the accumulation zone; (d) englacial ice at Victoria Flat; (e) englacial ice in the lower glacier; and (f) all longitudinal englacial samples (accumulation zone, Victoria Flat and lower glacier). Each plot shows the 95% confidence intervals about the least-squares linear regression model and corresponding R^2 values.

Table 3. Statistics for best-fit linear regression relationships between δD and $\delta^{18}O$

Facies	Regression model	b_1 (95% range)	R^2	F	p
Basal ice	$\delta D = 6.330\delta^{18}O - 5.014$	6.330 (5.304–7.381)	0.93	212.69	<0.001
Shear plane ice	$\delta D = 7.917\delta^{18}O + 10.156$	7.917 (5.665–10.834)	0.74	40.171	<0.001
Firn	$\delta D = 7.869\delta^{18}O + 7.986$	7.869 (5.366–10.597)	0.76	45.91	<0.001
Englacial (Victoria Flat)	$\delta D = 5.065\delta^{18}O - 16.546$	5.065 (2.331–7.119)	0.68	21.97	<0.001
Englacial (lower glacier)	$\delta D = 7.672\delta^{18}O + 7.392$	7.672 (6.788–8.701)	0.97	373.61	<0.001
Englacial (longitudinal)	$\delta D = 6.827\delta^{18}O - 0.959$	6.827 (6.230–7.435)	0.93	526.79	<0.001

The 95% range for b_1 ($\delta^{18}O$) coefficient is calculated as the mean ±2 standard errors of the estimate. p is the significance level at which R^2 and F are significant.

glaciers, with large accumulation zones and steep long profiles (Hambrey and Lawson, 2000). The primary stratification (S_0) evident across the accumulation zone is then tilted and deformed by transport from this broad névé into the narrow trunk, and then via flow through the upper and lower icefalls. Foliation (S_1) is a pervasive planar structure found in almost all glaciers (Hambrey and Lawson, 2000), and at Fox Glacier, it is tilted at high angles as isoclinal fold limbs. It is visible across the glacier surface as alternating layers of bubble-rich and bubble-free ice, formed under laterally compressive and longitudinally tensile stresses (Hambrey, 1975), and 'transposes' the original primary stratification (S_0). Indeed, foliation does not appear to cross-cut primary stratification, implying that foliation evolves from primary stratification (Roberson, 2008). Both crevasses and crevasse traces (S_2) are ubiquitous features of most glaciers (Hambrey and others, 2005), with the style of crevassing in Fox Glacier typical of alpine valley glaciers. Indeed, zones of extending flow (Herman and others, 2011) cause crevassing to develop in the upper and lower icefalls. Chevron and splaying crevasses are prevalent toward the glacier margins, caused by friction with the valley side (Benn and Evans, 2010), and transverse crevasses in areas of longitudinal extension, such as above icefalls. Longitudinal crevasses also develop at Victoria Flat, and near the terminus, due to the wider valley floor accommodation space, allowing lateral extension. Arcuate, up-glacier dipping debris-bearing shear planes (S_3) near the terminus have been interpreted previously by Appleby and others (2010) to represent longitudinal shortening and possible thrusting.

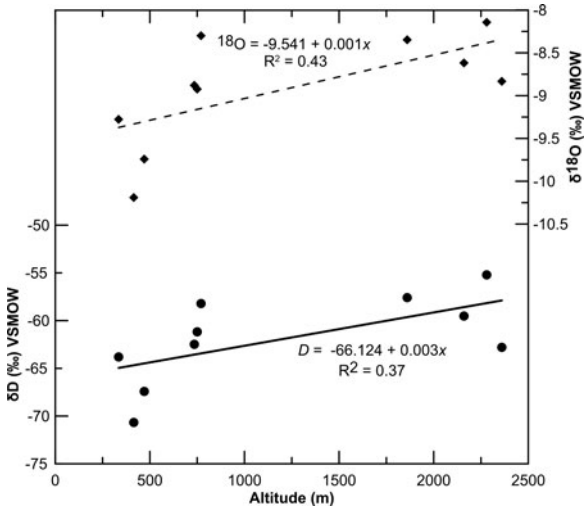

Fig. 7. Altitudinal variation in mean $\delta^{18}O$ (top) and δD (bottom) from samples along the longitudinal transect at Fox Glacier.

For most of ice facies (apart from englacial samples at Victoria Flat), the stable isotope samples approximate the LMWL, with a δD–$\delta^{18}O$ slope of 6.8 and 7.7 for Fox Glacier and Invercargill, respectively. The slope of the firn facies (S_0) samples (7.9) is particularly close to the monthly GNIP data at Invercargill, indicating that the névé has not undergone significant isotopic modification since direct snowfall. Although strong spatial variability in the isotopic composition of precipitation occurs across New Zealand, leading to more enriched δD–$\delta^{18}O$ values northwards (Barbour, 2007; Amesbury and others, 2015), both Fox Glacier and Invercargill are in a cooler climate, more dominated by the prevailing southern ocean westerly winds.

It is important to contextualize these results, as the isotopic composition of ice and firn is usually used in glaciology to interpret the formational history of glacier ice and firn, as well as debris entrainment mechanisms (Souchez and Jouzel, 1984; Souchez and de Groote, 1985; Lawson and others, 1998; Glasser and others, 2003). While some previous studies have focused on temperate glaciers (Epstein and Sharp, 1959; Sharp and others, 1960; Hambrey, 1974; Lawson and Kulla, 1978; Lemmens and others, 1982; Stichler and others, 1982; Goodsell and others, 2005; Swift and others, 2006; Cook and others, 2010), few, if any, previous studies have focused on mid-latitude, temperate maritime alpine glaciers. This provides limited scope for interpreting the thermal history of glacier ice at Fox Glacier in the context of directly comparable previous work. Nevertheless, in comparison with Purdie and others (2010) at adjacent Franz Josef Glacier, both the 94 δD and $\delta^{18}O$ values sampled from the different facies and locations at Fox Glacier span a relatively small range, between −54.92 to −71.83‰, and −7.97 to −10.33 for δD and $\delta^{18}O$, respectively. These data closely correspond to the data ranges reported by Purdie and others (2010) for Franz Josef Glacier snowfall data, which span from −9.38 to −14.28 (mean −14.28) for $\delta^{18}O$, and from −57.80 to −177.30 (mean −102.04) for δD (Purdie and others, 2010: p. 4742). The Fox Glacier ice facies isotope data generally show more positive values than the Franz Josef snowfall data, suggestive of fractionation.

Indeed, since water undergoes isotopic fractionation on freezing, measurements of δD–$\delta^{18}O$ can be used to distinguish between isotopically unmodified surface glacier ice and isotopically modified basal ice (Souchez and Jouzel, 1984; Lehmann and Siegenthaler, 1991; Glasser and others, 2003; Moore and others, 2013; Lovell and others, 2015a, b). The stable isotope composition of the shear plane ice samples (S_3) shows more positive values when compared with the juxtaposed clean ice in the lower glacier, indicating that freezing of interstitial ice water as

the debris was elevated from the subglacial zone has occurred (Moore and others, 2013). Indeed, this is consistent with ice formation through refreezing of water in close association with a debris-rich bed, as reported by other authors (Lawson, 1979; Hubbard and Sharp, 1993; Iverson and Souchez, 1996). Basal ice sampled at the glacier margin also appears slightly more enriched than englacial ice sampled at Victoria Flat and the lower glacier, the latter being particularly depleted. This contrasts with the surrounding englacial ice sampled in Victoria Flat and the ablation zone, which is interpreted at meteoric ice formed by the firnification of snow in the glacier's accumulation area, with the alternating bubble-poor and bubble-rich layers reflecting seasonal melting and refreezing (cf. Hambrey, 1975).

Despite this, the co-isotope plots, along with subsample means and SDs of each sample facies, suggest that there are only subtle differences between ice facies. The relative 'homogenization' of co-isotope values across the different sample facies may have resulted from isotopic modification of the snowpack during the transformation from firn to ice, perhaps through the percolation of surface meltwater, or from melting/refreezing events within the snowpack itself (Glasser and Hambrey, 2002). Samples of glacier ice that have not undergone refreezing should lie along the same regression line as precipitation (normally with a slope of ~8) when plotted on a δD–$\delta^{18}O$ diagram. However, plotting the means and SD of the Fox Glacier facies together, there is only a subtle differentiation between the different ice types, although all show enrichment relative to the Franz Josef Glacier winter snowfall data reported in Purdie and others (2010). This suggests that the ice facies in general have a common origin. Neither the coarse-bubbly ice facies, the coarse-clear ice facies, nor the debris-rich clotted ice in the shear planes (S_3) appear to have clearly undergone isotopic fractionation by the incomplete freezing of available water (see Lawson and others, 1998). Hence, invoking processes of melting and refreezing in one ice facies relative to another is problematic with the Fox Glacier dataset.

An additional issue at glaciers, such as Fox Glacier, in interpreting δD–$\delta^{18}O$ values is caused by the heavily crevassed regions in the ablation zone, which reach near or fully to the glacier bed. Hence, the amount of rainwater able to reach the subglacial drainage system, and in turn melt subglacial ice via advection of the relatively warm water, will be high (Alexander and others, 2011).

The stable isotope data outlined above, along with surface observations and the time-lapse imagery of the terminus, clearly have implications for debris entrainment and transfer. Debris entrainment and thrusting has been cited by several authors as an important mechanism in transporting sediment upwards from the bed. Most researchers who invoke thrusting suggest that hanging walls of fast-sliding ice are thrusted over footwalls of stagnant or slow-moving marginal ice in a longitudinally compressive environment at glacier termini (cf. Hudleston, 2015). Despite its widespread application, the thrust model for the uplift of basal debris, and criteria for the field recognition of thrusts, is debated (Weertman, 1961; Hooke and Hudleston, 1978; Woodward and others, 2002; Glasser and others, 2003; Rea and Evans, 2011). While Weertman (1961) argued that sediment transfer along thrusts would be inefficient, a growing body of work from polythermal glaciers in Svalbard (Glasser and others, 1998, 1999; Glasser and Hambrey, 2001) and Storglaciaren, Sweden (Moore and others, 2010, 2011, 2013) indicates that thrusting can be an important mode of elevating basal and glaciofluvial debris to the ice surface from subglacial and englacial positions. Work on alpine glaciers in the European Alps (Goodsell and others, 2005; Herbst and others, 2006) reported accumulations of basal material similar to that described at Fox Glacier on the surface of Pasterzenkees, Austria and Haut Glacier d'Arolla, Switzerland. Three glaciotectonic processes likely to elevate debris to the surface have been proposed by Glasser and others (2003): (1) large-scale recumbent folding, (2) compression caused by a thermal boundary between a thawed and deforming bed and (3) over-riding of ice-marginal stagnant ice. These proposals are rejected for Fox Glacier on the basis of observations herein, together with the high ice velocities at the terminus (~1 m d^{-1}; Purdie and others, 2008), and the meltwater availability. Instead, a model of thrusting caused by the glacier advancing into an aggraded proglacial foreland (Herbst and others, 2006), according to the observed structural characteristics, would appear to be a more realistic scenario.

These results have highlighted the range in meteoric-derived water stable isotopic compositions within New Zealand's dynamic maritime climate system. Indeed, the ranges in δD at Fox Glacier are around one-half the range of δD values seen in the polar ice cores from the Last Glacial Maximum (LGM) to the late Holocene (Winter and others, 2016). Hence, these ranges in maritime alpine glacier stable isotopic compositions make them potentially useful targets for tracing glacier deformation processes, if careful isotope sampling from clearly established ice facies identified within the glacier system (Hudleston, 2015) is undertaken.

CONCLUSIONS

Evidence for flow dynamics and deformation at Fox Glacier, a temperate, mid-latitude maritime glacier are evident from time-lapse imagery, surface observations and stable isotope sampling in 2010/11, at the end of the most recent period of advance (1984–2009). The stable isotopes show contrasts between the debris-bearing shear plane facies and values typical of clean englacial facies. In common with many other alpine valley glaciers with a high AAR, ice is highly deformed due to topographic constriction within a channelized valley, in addition to a steep, undulating long profile. The sequential development of structures within the glacier consists of: (1) the formation of primary stratification through firnification processes in the accumulation area; (2) folding of primary stratification to produce longitudinal foliation; (3) opening of extensional fractures and crevasses, some of which close to form crevasse traces; (4) arcuate debris-bearing shear planes close to the terminus due to longitudinal compression, with apparent hanging wall and footwall fault blocks, characteristic of thrust faulting.

The stable isotope samples are plot on a line with a slope of 6.8 on a co-isotopic plot of δD and $\delta^{18}O$. This line closely approximates the LMWL (7.7) obtained from monthly precipitation data collected by the IAEA at Invercargill, at the southern tip of the South Island. Moreover, the slope of the Fox Glacier névé samples (7.9) is particularly close to the monthly LMWL data at Invercargill, indicating that the névé has not undergone significant isotopic modification from direct snowfall. In addition, all of the Fox Glacier facies sampled either overlap, or are close to the maximum values of the isotope data reported in a prior study of winter snowfall on the adjacent Franz Josef Glacier. Comparing the

co-isotopic plot slope gradients and regression statistics shows that some slopes are less steep than others, with the shear plane ice at the terminus having the steepest line (7.9), and Victoria Flat englacial facies having the lowest gradient (5.1). However, the difference in these relationships was not statistically different, given the limited sample sizes. Nevertheless, the stable isotope composition of the shear plane ice facies shows slightly more positive values when compared with the nearby englacial ice samples, indicating that freezing of interstitial water has occurred as the debris was elevated from the subglacial zone. This accords with ice formation through refreezing of water in close association with a debris-rich bed, as reported elsewhere.

ACKNOWLEDGEMENTS

Discussions in the field at Fox Glacier with Mike Hambrey (University of Aberystwyth) and Peter Barrett (Victoria University of Wellington) is gratefully acknowledged. The research was funded by Massey University Research Funding (MURF) to M.S.B., and a Vice Chancellor's Massey University PhD Scholarship to J.R.A.. We are indebted to the very detailed comments of an anonymous reviewer, who helped to substantially improve this paper.

REFERENCES

Alexander DJ, Shulmeister J and Davies T (2011) High basal melting rates within high-precipitation temperate glaciers. *J. Glaciol.*, **57**, 789–795

Alley RB and 5 others (1997) How glaciers entrain and transport basal sediment; physical constraints. *Quat. Sci. Rev.*, **16**, 1017–1038

Amesbury MJ and 10 others (2015) Can oxygen stable isotopes be used to track precipitation moisture source in vascular plant-dominated peatlands? *Earth Planet. Sci. Lett.*, **430**, 149–159

Appleby JR, Brook MS, Vale SS and MacDonald-Creevey AM (2010) Structural glaciology of a temperate maritime glacier: lower Fox Glacier, New Zealand. *Geogr. Ann.*, **92**(A), 451–467

Barbour MM (2007) Stable oxygen isotope composition of plant tissue: a review. *Funct. Plant Biol.*, **34**, 83–94

Benn DI and Evans DJA (2010). *Glaciers and glaciation*. Hodder Arnold, London, 734 p

Brook M and Paine S (2012) Ablation of ice-cored moraine in a humid, maritime climate: Fox Glacier, New Zealand. *Geogr. Ann.*, **94A**, 339–349

Coates G and Chinn TJ (1999) *The Franz Josef and fox glaciers*. Institute of Geological and Nuclear Sciences Ltd, Wellington

Cook SJ and 5 others (2010) Role of glaciohydraulic supercooling in the formation of stratified facies basal ice: Svínafellsjökull and Skaftafellsjökull, southeast Iceland. *Boreas*, **39**(1), 24–38

Epstein S and Sharp RP (1959) Oxygen isotope variations in the Malaspina and Saskatchewan Glaciers. *J. Geol.*, **67**, 88–102

Fierz C and 8 others (2009) *The international classification for seasonal Firn on the ground*. IHP-VII Technical Documents in Hydrology No.83, IACS Contribution No.1, UNESCO-IHP, Paris

Glasser NF and Hambrey MJ (2001) Styles of sedimentation beneath Svalbard valley glaciers under changing dynamic and thermal regimes. *J. Geol. Soc. Lond.*, **158**, 697–708

Glasser NF and Hambrey MJ (2002) δD–$\delta^{18}O$ relationships on a polythermal valley glacier: Midtre Lovénbreen, Svalbard. *Polar Res.*, **21**, 123–131

Glasser NF, Hambrey MJ, Crawford KR, Bennett MR and Huddart D (1998) The structural glaciology of Kongsvegen, Svalbard and its role in landform genesis. *J. Glaciol.*, **44**, 136–148

Glasser NF, Bennett MR and Huddart D (1999) Distribution of glaciofluvial sediment within and on the surface of a high Arctic valley glacier: Marthabreen, Svalbard. *Earth Surf. Process. Landf.*, **24**(4), 303–318

Glasser NF, Hambrey MJ, Etienne JL, Jansson P, and Pettersson R (2003) The origin and significance of debris-charged ridges at the surface of Storglaciären, northern Sweden. *Geogr. Ann.*, **85A**, 127–147

Gonfiantini R (1978) Standard for stable isotope measurements in natural compounds. *Nature*, **271**, 534–536

Goodsell B, Hambrey MJ and Glasser NF (2005) Debris transport in a temperate valley glacier: Haut Glacier d'Arolla, Valais, Switzerland. *J. Glaciol.*, **51**, 139–146

Hambrey MJ (1974) Oxygen isotope studies at Charles Rabots Bre, Okstindan, northern Norway. *Geogr. Ann.*, **56A**, 147–159

Hambrey MJ and Lawson W (2000) Structural styles and deformation fields in glaciers: a review. In Maltman AJ, Hubbard B and Hambrey MJ eds. *Deformation of glacial materials, Geol. Soc. Spec. Publ.*, **176**, 56–83

Hambrey MJ (1975) The origin of foliation in glaciers: evidence from some Norwegian examples. *J. Glaciol.*, **14**(70), 181–185

Hambrey MJ, Bennett MR, Dowdeswell JA, Glasser NF and Huddart D (1999) Debris entrainment and transfer in polythermal valley glaciers. *J. Glaciol.*, **45**, 69–86

Hambrey MJ and 7 others (2005) Structure and changing dynamics of a polythermal valley glacier on a centennial timescale: Midre Lovenbreen, Svalbard. *J. Geophys. Res.*, **110**, F01006 (doi: 10.1029/2004JR000128)

Herbst P, Neubauer F and Schopfer MPJ (2006) The development of brittle structures in an alpine valley glacier: Pasterzenkees, Austria, 1887–1997. *J. Glaciol.*, **52**(176), 128–136

Herman F, Anderson B and LePrince S (2011) Mountain glacier velocity variation during an advance/retreat cycle quantified using sub-pixel analysis of ASTER images. *J. Glaciol.*, **57**(202), 197–207

Hooke RL and Hudleston PJ (1978) Origin of foliation in glaciers. *J. Glaciol.*, **20**, 285–299

Hubbard B and Sharp M (1993) Weertman regelation, multiple refreezing events and the isotopic evolution of the basal ice layer. *J. Glaciol.*, **39**(132), 275–291

Hubbard B, Tison J-L, Janssens L, and Spiro B (2000) Ice-core evidence of the thickness and character of clear-facies basal ice: Glacier de Tsanfleuron, Switzerland. *J. Glaciol.*, **46**(152), 140–150

Hubbard B, Cook S and Coulson H (2009) Basal ice facies: a review and unifying approach. *Quat. Sci. Rev.*, **28**, 1956–1969

Hudleston PJ (2015). Structures and fabrics in glacial ice: a review. *J. Struct. Geol.*, **81**, 1–27

IAEA (1992) Statistical treatment of data on environmental isotopes in precipitation. Technical Reports Series No. 331, IAEA, Vienna, p. 781

Iverson NR and Souchez R (1996) Isotopic signature of debris-rich ice formed by regelation into a subglacial sediment bed. *Geophys. Res. Lett.*, **23**(10), 1151–1154

Jennings SJA, Hambrey MJ and Glasser NF (2014) Ice flow-unit influence on glacier structure, debris entrainment and transport. *Earth Surf. Process. Landf.*, **39**, 1279–1292

Larsen NK, Kronborg C, Yde JV and Knudsen NT (2010) Debris entrainment by basal freeze-on and thrusting during the 1995–1998 surge of Kuannersuit Glacier on Disko Island, west Greenland. *Earth Surf. Process. Landf.*, **35**(5), 561–574

Lawson DE (1979) Sedimentological analysis of the western terminus region of the Matanuska Glacier, Alaska. *CRREL Rep.*, 79–97

Lawson DE and Kulla JB (1978) An oxygen isotope investigation of the origin of the basal zone of the Matanuska Glacier, Alaska. *J. Geol.*, **86**, 673–685

Lawson DE and 5 others (1998) Glaciohydraulic supercooling: a freeze-on mechanism to create stratified, debris-rich basal ice: I. Field evidence. *J. Glaciol.*, **44**, 547–562

Lehmann M and Siegenthaler U (1991) Equilibrium oxygen and hydrogen-isotope fractionation between ice and water. *J. Glaciol.*, **37**, 23–26

Lemmens M, Lorrain R and Haren J (1982) Isotopic composition of ice and subglacially precipitated calcite in an alpine area. *Z. Gletscherkd. Glazialgeol.*, **18**, 151–159

Lovell H and 5 others (2015a) Former dynamic behaviour of a cold-based valley glacier on Svalbard revealed by basal ice and structural glaciology investigations. *J. Glaciol.*, **61**(226), 309–328

Lovell H and 8 others (2015b) Debris entrainment and landform genesis during tidewater glacier surges. *J. Geophys Res.: Earth Surf.*, **120**, 1574–1595

Moore PL, Iverson NR and Cohen D (2010) Conditions for thrust faulting in a glacier. *J. Geophys. Res.: Earth Surf.*, **115**(F02005)

Moore PL and 5 others (2011) Effect of a cold margin on ice flow at the terminus of Storglaciaren, Sweden: implications for sediment transport. *J. Glac.*, **57**(201), 77–87

Moore PL and 5 others (2013) Entrainment and emplacement of englacial debris bands near the margin of Storglaciaren, Sweden. *Boreas*, **42**, 71–83

Phillips E, Finlayson A and Jones L (2013) Fracturing, block faulting, and moulin development associated with progressive collapse and retreat of a maritime glacier: Falljökull, SE Iceland. *J. Geophys Res.: Earth Surf.*, **118**, 1545–1561

Purdie HL, Brook MS and Fuller IC (2008) Seasonal variation in ablation and surface velocity on a temperate maritime Glacier: Fox Glacier, New Zealand. *Arct. Antarct. Alp. Res.*, **40**(1), 140–147

Purdie H, Bertler N, Mackintosh A, Baker J and Rhodes R (2010) Isotopic and elemental changes in winter snow accumulation on glaciers in the Southern Alps of New Zealand. *J. Clim.*, **23**(18), 4737–4749

Purdie H and 5 others (2014) Franz Josef and Fox Glaciers, New Zealand: historic length records. *Glob. Plan. Chan.*, **121**, 41–52

Rea BR and Evans DJ (2011) An assessment of surge-induced crevassing and the formation of crevasse squeeze ridges. *J. Geophys Res.: Earth Surf.*, **116**(F04005)

Roberson S (2008) Structural composition and sediment transfer in a composite cirque glacier: Glacier de St. Sorlin, France. *Earth Surf. Proc. Landf.*, **33**(13), 1931–1947

Sharp M, Jouzel J, Hubbard B and Lawson W (1994) The character, structure and origin of the basal ice layer of a surge-type glacier. *J. Glaciol.*, **40**(135), 327–340

Sharp RP, Epstein S and Vidziunas I (1960) Oxygen isotope ratios in Blue Glacier, Olympic Mountains, Washington. *J. Geophys. Res.*, **65**, 4043–4059

Souchez RA and de Groote JM (1985) δD–δ18O relationships in ice formed by subglacial freezing: palaeoclimatic implications. *J. Glaciol.*, **31**, 229–232

Souchez RA and Jouzel J (1984) On the isotopic composition in δD and $\delta^{18}O$ of water and ice during freezing. *J. Glaciol.*, **30**(106), 369–372

Stichler W, Baker D, Oerter H and Trimborn P (1982) Core drilling on Vernagtferner (Oetztal Alps, Austria) in 1979: deuterium and oxygen-18 contents. *Z. Gletscherkd. Glazialgeol.*, **18**, 23–35

Swift DA, Evans DJA and Fallick AE (2006) Transverse englacial debris-rich ice bands at Kviarjokull, southeast Iceland. *Quat. Sci. Rev.*, **25**(13–14), 1708–1718

Wardle P (1973) Variations of the glaciers of Westland National Park and the Hooker Range, New Zealand. *NZ J. Botany*, **11**, 349–388

Weertman J (1961) Stability of ice-age ice sheets. *J. Geophys. Res.*, **66**, 3783–3792

Winter K and 10 others (2016) Assessing the continuity of the blue ice climate record at Patriot Hills, Horseshoe Valley, West Antarctica. *Geophys. Res. Lett.*, **43**(5), 2019–2026

Woodward J, Murray T and McCaig A (2002) Formation and reorientation of structure in the surge-type glacier Kongsvegen, Svalbard. *J. Quat. Sci.*, **17**, 201–209